Universiteit Leiden
The Netherlands

PI3K signaling and adherens junctions in invasive lobular breast cancer

Klarenbeek, S.

Citation

Klarenbeek, S. (2021, April 15). *PI3K signaling and adherens junctions in invasive lobular breast cancer*. Retrieved from https://hdl.handle.net/1887/3154437

Version:	Publisher's Version
License:	Licence agreement concerning inclusion of doctoral thesis in the Institutional Repository of the University of Leiden
Downloaded from:	https://hdl.handle.net/1887/3154437

Note: To cite this publication please use the final published version (if applicable).

Cover Page

Universiteit Leiden

Leiden University Repository

The handle http://hdl.handle.net/1887/3154437 holds various files of this Leiden University dissertation.

Author: Klarenbeek, S.
Title: PI3K signaling and adherens junctions in invasive lobular breast cancer
Issue date: 2021-04-15

3

A preclinical mouse model of invasive lobular breast cancer metastasis

Chris W. Doornebal[1,3,4], Sjoerd Klarenbeek[2,3], Tanya M. Braumuller[2,3], Christiaan N. Klijn[2,3], Metamia Ciampricotti[1,3], Cheei-Sing Hau[1,3], Markus W. Hollmann[4], Jos Jonkers[2,3], and Karin E. de Visser[1,3]

[1] Division of Immunology, Netherlands Cancer Institute, Amsterdam, The Netherlands
[2] Division of Molecular Pathology, Netherlands Cancer Institute, Amsterdam, The Netherlands
[3] Cancer Systems Biology Center, Netherlands Cancer Institute, Amsterdam, The Netherlands
[4] Department of Anesthesiology, Academic Medical Center, Amsterdam, the Netherlands

Cancer Research 73, 353-363 (2013)

ABSTRACT

Metastatic disease accounts for more than 90% of cancer-related deaths, but the development of effective antimetastatic agents has been hampered by the paucity of clinically relevant preclinical models of human metastatic disease. Here, we report the development of a mouse model of spontaneous breast cancer metastasis, which recapitulates key events in its formation and clinical course. Specifically, using the conditional *K14cre;Cdh1*$^{F/F}$*;Trp53*$^{F/F}$ model of *de novo* mammary tumor formation, we orthotopically transplanted invasive lobular carcinoma (mILC) fragments into mammary glands of wild-type syngeneic hosts. Once primary tumors were established in recipient mice, we mimicked the clinical course of treatment by conducting a mastectomy. After surgery, recipient mice succumbed to widespread overt metastatic disease in lymph nodes, lungs, and gastrointestinal tract. Genomic profiling of paired mammary tumors and distant metastases showed that our model provides a unique tool to further explore the biology of metastatic disease. Neoadjuvant and adjuvant intervention studies using standard-of-care chemotherapeutics showed the value of this model in determining therapeutic agents that can target early- and late-stage metastatic disease. In obtaining a more accurate preclinical model of metastatic lobular breast cancer, our work offers advances supporting the development of more effective treatment strategies for metastatic disease.

INTRODUCTION

Metastasis formation is a complex and dynamic process in which cancer cells escape the primary tumor and disseminate to secondary organs by successfully advancing through a sequence of several steps. After initial invasion of the extracellular matrix, cancer cells intravasate into blood and lymphatic vasculature, survive during transit, and extravasate to colonize distant organs (1–3). Despite recent advances, many of the mechanisms by which cancer cells acquire the ability to overcome each of these successive barriers remain poorly understood. Furthermore, a growing body of evidence indicates that metastasis formation is influenced by a continuous crosstalk between cancer cells and their stromal environment (4). For example, organ-specific patterns of metastatic spread observed in distinct subtypes of cancer strongly suggest that host factors play a critical role in the dissemination of cancer cells (5). This notion is further supported by the observation of chemokine-mediated trafficking of circulating tumor cells to distant sites (6). Recent studies also suggest that tumor-derived factors can facilitate metastatic colonization by recruiting bone marrow-derived hematopoietic progenitor cells to secondary sites, where these cells prime their environment to form a more hospitable and survival-permissive premetastatic niche (7–9).

To study metastasis formation *in vivo*, several mouse models of metastatic disease have been developed. Unfortunately, most of the currently available models only partially reflect the metastatic cascade. For example, experimental metastasis models based on intravenous injection of cancer cells do not recapitulate tumor cell invasion and intravasation, but only reflect homing of circulating tumor cells to an often limited set of secondary organs (10, 11). These issues are partially resolved in syngeneic or xenograft tumor transplantation models in which tumor cells derived from an established cancer cell line are transplanted subcutaneously or orthotopically into recipient mice. Xenograft metastasis models, which carefully reflect cancer-cell intrinsic traits of parental human carcinomas, are easily manipulated for mechanistic studies and have been particularly useful to evaluate therapeutic compounds targeting metastatic disease (12). However, *in vitro* maintained cancer cell lines fail to retain the cellular heterogeneity originally found in the parental tumor (13). Therefore, phenotypic variations in metastatic capacity that are present in spontaneous tumors are generally not recapitulated in cancer cell line–based metastasis models. Furthermore, xenograft metastasis models cannot be used to study the role of the adaptive immune system in disease progression and metastasis formation.

A third alternative to study metastasis formation *in vivo* is the use of mouse models of *de novo* tumorigenesis. Using these spontaneous mouse models to study metastatic dissemination offers several advantages over the previously described experimental systems (11). First, tumors derived from genetically engineered mouse (GEM) models often closely recapitulate the histopathologic characteristics observed in human cancer. Furthermore, tissue-specific induction of mutations gives rise to orthotopic tumors in the context of a functional, immune competent microenvironment, thus recapitulating the crosstalk between an emerging tumor and its surroundings. Consequently, mouse models of *de novo* tumorigenesis are useful to study early stages of metastatic spread and to explore the role of the stromal microenvironment in disease progression. Nonetheless, studying advanced metastatic disease in GEM models is often hampered by the relatively low incidence of metastatic disease. Even if metastatic dissemination occurs, most animals will, unlike in human cancer, die from rapidly growing primary tumors that do not allow sufficient time for the emergence of advanced, clinically overt metastatic disease. Though these issues could be resolved by surgical resection of the primary tumor, this often proves unpractical as most animals develop multiple, asynchronously arising primary tumors (12).

To address this caveat, we set out to develop a novel, preclinical mouse model of spontaneous breast cancer metastasis by exploiting the well-characterized conditional *K14cre;Cdh1*$^{F/F}$*;Trp53*$^{F/F}$ mouse model of *de novo* mammary tumor formation (14). Our main aim was to design a clinically relevant mouse model that recapitulates invasive lobular breast cancer metastasis in humans and represents all major events of the metastatic cascade. In addition, metastatic disease should develop spontaneously in a variety of biologically relevant organs, at a high penetrance and within a reasonable, predictable time frame rendering it a suitable preclinical mouse model to study the biology of metastatic disease as well as to test novel therapeutic agents targeting metastatic disease.

MATERIALS AND METHODS

Mice

The generation and characterization of *K14cre;Cdh1*$^{F/F}$*;Trp53*$^{F/F}$ mice, back-crossed onto the FVB/N background for this study, has previously been described in detail (14). Genotyping was conducted by PCR analysis on tail tip DNA as described previously (14). Female FBV/N mice (aged 10–12 weeks) were bred at and obtained from the laboratory animal facility at the Netherlands Cancer Institute (Amsterdam, the Netherlands). Mice

were kept in individually ventilated (intervention studies) and open cages (all other experiments) and food and water were provided *ad libitum*. Mouse handling and animal experimental procedures were approved by the Institute's Animal Ethics Committee and were conducted in accordance with Institutional guidelines and National Ethical Regulations.

Isolation of mammary donor tumors

In *K14cre;Cdh1$^{F/F}$;Trp53$^{F/F}$* females, the onset of mammary tumor formation was monitored twice weekly by palpation starting at 4 months of age. Mammary tumor growth was measured using calipers. Once mammary tumors reached a size of approximately 10 × 10 mm, tumors were harvested and cut in small pieces (diameter ~1 mm) while submerged in ice-cold PBS. Tumor fragments were collected by centrifugation at 1,200 rpm for 5 minutes, resuspended in Dulbecco's Modified Eagle's Medium F12 containing 30% fetal calf serum and 10% dimethyl sulfoxide and stored at −150 °C till further use.

Orthotopic tumor transplantations

On the basis of immunohistochemical stainings, 3 *K14cre;Cdh1$^{F/F}$;Trp53$^{F/F}$* derived mouse invasive lobular carcinomas (mILC), characterized by high cytokeratin 8 and absence of vimentin and E-cadherin expression, isolated from 3 independent mice were selected and used as donor tumors. Small tumor fragments (~1 mm in diameter) from these donor mILCs were orthotopically transplanted into the mammary fat pad of 10 week old wild-type syngeneic female recipients as described previously (15). Briefly, recipient animals were anesthetized by injecting a 7 mL/kg bolus of a 1:1:2 mixture of Hypnorm (Janssen Pharmaceutica): Dormicum (Roche): ddH_2O intraperitoneally. After shaving and disinfection, a midline abdominal incision of 1 cm was made at the level of the fourth nipple, and a small pocket was created by puncturing the mammary fat pad using watchmaker's forceps. A tumor fragment was inserted distal to the local lymph node, the mammary gland was repositioned, skin was stitched, and buprenorfine (100 µg/kg) was administered subcutaneously for postoperative pain relief.

Surgical resection of mammary tumors

The first occasion at which a tumor mass of approximately 2 × 2 mm was identified was defined as the time of diagnosis. Tumor growth was measured twice weekly using calipers. Once recipient mammary tumors reached a size of approximately 15 × 15 mm, a mastectomy was conducted. After induction of anesthesia and disinfection, a 2 cm

midline abdominal skin incision was made and tumor-supplying arteries were located and ligated. The mammary tumor including adjacent fourth and fifth mammary glands were separated from adherent tissues using forceps and soaked cotton swabs, and the mammary tumor was excised and stored for further analysis. The skin was closed using stitches and buprenorfine (100 µg/kg) was given for postoperative analgesia.

Monitoring of metastatic disease

Following mastectomy, all mice were monitored for disease progression and metastasis formation by palpation and daily observation of their physical health, appearance, and behavior. Recipient animals were sacrificed when they developed clinical signs of distress caused by metastatic disease, that is, respiratory distress (labored breathing as a result of lung metastases and pleural effusion leading to a reduced respiratory capacity), ascites, distended abdomen, rapid weight gain and severe anemia (associated with liver metastases), and palpable metastatic lesions in lymphoid organs, or suffered from locally relapsing tumors that reached a size of approximately 15 × 15 mm. Brain, lungs, liver, spleen, intestines, mesenterium, kidneys, adrenal glands, ovaries, uterus, mammary glands, left femur, sternum, and tumor-draining and distant lymph nodes (mesenteric, renal, and caudal) were collected and analyzed microscopically for the presence of metastatic foci. Macroscopically overt metastases were collected separately for further analysis.

Histopathologic and genomic characterization of mammary tumors and metastases

Mammary tumors and metastases were characterized by histopathologic, immunohistochemical, and array comparative genomic hybridization (aCGH) analyses. Detailed methods are described in Supplementary Material.

Neoadjuvant and adjuvant chemotherapy treatments

To study chemotherapy responses in mammary tumors and distant metastases, we generated a cohort of recipient mice transplanted with the same donor tumor (donor tumor 1). Tumor-bearing recipients were assigned to adjuvant or neoadjuvant treatments with PBS (control), doxorubicin (5 $mg.kg^{-1}$), or docetaxel (22 $mg.kg^{-1}$) intravenously (tail vein injection) at maximum tolerable doses. Adjuvant and neoadjuvant treatments were administered once weekly for a fixed period of 4 weeks. Neoadjuvant intervention studies were initiated as soon as mammary tumors reached a size of 5 × 5 mm. Following mastectomy at a tumor size of approximately 15 × 15 mm, neoadjuvant treated mice were monitored for disease progression as described previously. Adjuvant treated

recipients underwent a mastectomy once the mammary tumor reached a size of 15 × 15 mm. Adjuvant treatments were initiated 3 days after mastectomy according to the same treatment schedule. Therapeutic profiles of mammary tumors and distant metastases were studied using mammary tumor growth (neoadjuvant setting only) and metastasis-specific survival (both settings) as primary endpoints.

Statistical analysis

Array CGH data analyses were conducted in *R* using the comparative module of the *Kcsmart* (16, 17) as implemented in the *Bioconductor* toolbox (version 2.8). All other data analyses were conducted in GraphPad Prism version 5.01 (GraphPad Software Inc). Applied analyses are indicated in corresponding legends when appropriate.

RESULTS

Transplantation of spontaneous K14cre;Cdh1$^{F/F}$;Trp53$^{F/F}$ derived mILCs results in outgrowth of clonally related and phenotypically similar recipient mammary tumors

To develop a novel, preclinical mouse model of spontaneous breast cancer metastasis formation, we used the conditional *K14cre;Cdh1$^{F/F}$;Trp53$^{F/F}$* mouse model of *de novo* mammary tumor formation previously described by Derksen and colleagues (14). *K14cre;Cdh1$^{F/F}$;Trp53$^{F/F}$* females spontaneously develop pleiomorphic mILCs based on stochastic loss of E-cadherin and p53 in mammary epithelium. These spontaneous mILCs resemble human invasive lobular carcinomas with respect to their histopathologic features as well as in their metastatic behavior (14, 18). Nonetheless, *K14cre;Cdh1$^{F/F}$;Trp53$^{F/F}$* mice do not succumb to clinically overt metastatic disease, but die due to independent, asynchronously arising, and rapidly growing primary tumors, thus hampering in depth analyses of metastatic disease in this spontaneous mouse model (12). To circumvent these limitations, we orthotopically transplanted small tumor fragments from 3 independent, spontaneous *K14cre;Cdh1$^{F/F}$;Trp53$^{F/F}$* derived mILCs into mammary glands of wild-type syngeneic hosts (Fig. 1A&B). To prolong survival and allow sufficient time for disseminated cancer cells to establish metastases, we mimicked the clinical setting and surgically resected recipient mammary tumors that reached a size of approximately 15 × 15 mm (Fig. 1A and C). Following mastectomy, we closely monitored recipient mice for clinical signs and symptoms of metastatic disease (Fig. 1A).

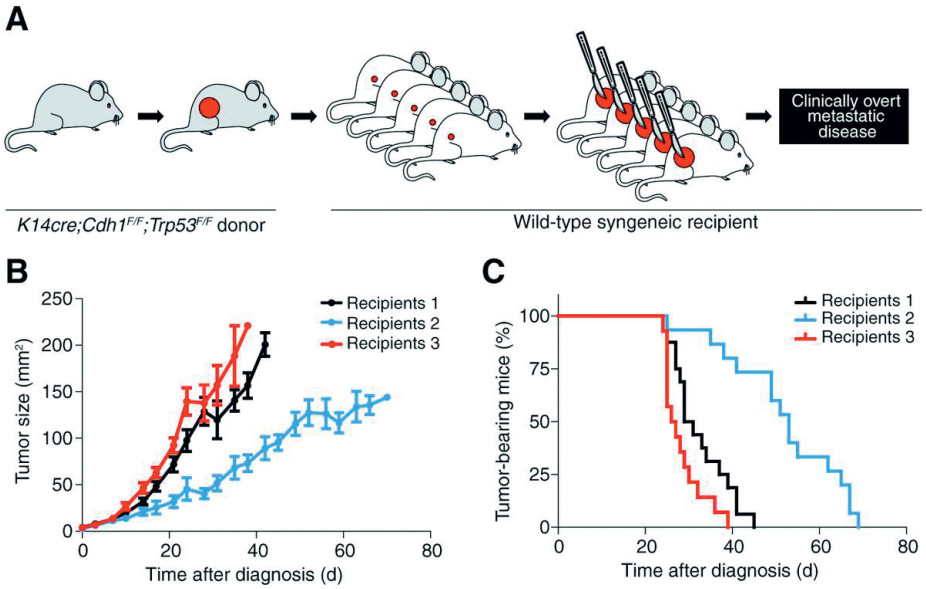

Figure 1. Overview of a preclinical mouse model of *de novo* breast cancer metastasis formation. A, small tumor fragments (~1 × 1 mm) derived from mILCs that spontaneously developed in *K14cre;Cdh1*$^{F/F}$*;Trp53*$^{F/F}$ mice (gray mice) are transplanted orthotopically into the fourth mammary gland of wild-type syngeneic recipient animals (white mice). Once recipient tumors reach a size of approximately 15 × 15 mm, mastectomy is conducted. Following surgery, mice are monitored for clinical signs and symptoms of metastatic disease. B, tumor growth kinetics in recipient mice transplanted with 3 independent donor mILCs. Tumor growth is depicted as tumor size (mean mm^2 ± SEM) over time, starting from the time of diagnosis (day 0), that is, the first occasion after transplantation at which a solid tumor mass of approximately 2 × 2 mm was identified (recipients 1, n = 16; recipients 2, n = 14; recipients 3, n = 14). C, Kaplan–Meier tumor latency curves of the same recipient animals as shown in B presenting the interval between diagnosis (day 0) and surgical resection of the primary tumor reaching a size of approximately 15 × 15 mm (defined as an event). d, days.

To first explore whether recipient mammary tumors were phenotypically similar to their parental tumor, we characterized donor and recipient mammary tumors by means of morphologic, immunohistochemical, and array comparative genomic hybridization (aCGH) studies. Mammary donor tumors were morphologically classified as solid, moderately invasive, pleiomorphic mILCs and uniformly expressed cytokeratin 8 (CK8), but did not express vimentin or E-cadherin (Fig. 2A, Top). Consistent with these observations, recipient mammary tumors derived from donor tumor 1 were mostly classified as solid, pleiomorphic mILCs and stained positive for CK8 and negative for vimentin and E-cadherin (Fig. 2A, Middle and Supplementary Fig. S1A). Yet, the majority of recipient tumors derived from donor mILCs 2 and 3 displayed a more heterogeneous, biphasic morphology (Fig. 2A, Bottom and Supplementary Fig. S1A). Though typical

epithelial regions were still present in these tumors, areas with a mesenchymal or spindle-like cell morphology characterized by pleiomorphic nuclei with densely packed chromatin and a small cytoplasm were also observed (Fig. 2A, bottom). These findings were further confirmed by immunohistochemistry, which revealed sharply delineated regions of CK8^{+}/vimentin^{-} and CK8^{-}/vimentin^{+} fields indicating a mixed composition of epithelial- and mesenchymal-like components within recipient outgrowths (Fig. 2A, Bottom). The sharply delineated epithelial- and mesenchymal-like areas suggest that these tumor cells originated from different, independent subclones of cancer cells that were present in the heterogeneous parental tumor. Like spontaneous donor tumors, recipient outgrowths were heavily infiltrated by T lymphocytes and macrophages (Supplementary Fig. S1B), which have been shown to play a prominent role in breast cancer metastasis (19–21). Together, these findings indicate that transplanted *K14cre;Cdh1$^{F/F}$;Trp53$^{F/F}$* derived mILC fragments give rise to recipient mammary tumors that closely resemble the histopathologic characteristics of the pleiomorphic parental tumor.

To examine the genomic relationship between donor and recipient mammary tumors, we conducted aCGH on recipient mammary tumors and their corresponding parental tumor. Genomic profiles of *de novo K14cre;Cdh1$^{F/F}$;Trp53$^{F/F}$* donor tumors were highly conserved in transplanted recipient outgrowths (Supplementary Fig. S2). Consistent with these observations, genomic profiles of recipient mammary tumors clustered according to their parental tumor (Fig. 2B). Together, these data indicate that transplantation of spontaneous *K14cre;Cdh1$^{F/F}$;Trp53$^{F/F}$* derived mILCs leads to reconstitution of clonally related recipient mammary tumors that conserve the genomic profile of the parental tumor.

Surgical resection of mammary tumors results in widespread clinically overt metastatic disease in recipient mice

To examine whether transplanted recipient mILCs maintain their capacity to disseminate and establish spontaneous metastases, we surgically resected recipient mammary tumors at a size of approximately 15 × 15 mm (Fig. 1A). Following mastectomy, 32 of 44 recipient mice succumbed to clinically overt metastatic disease in lungs (respiratory distress), liver (severe anemia, ascites accompanied by weight gain, and a distended abdomen), spleen (palpable tumor mass), and/or tumor-draining or distant lymph nodes (tumor mass reaching a size of ~15 × 15 mm; Fig. 3A). In addition, 12 of 44 recipient mice died due to locally relapsing tumors (Fig. 3A).

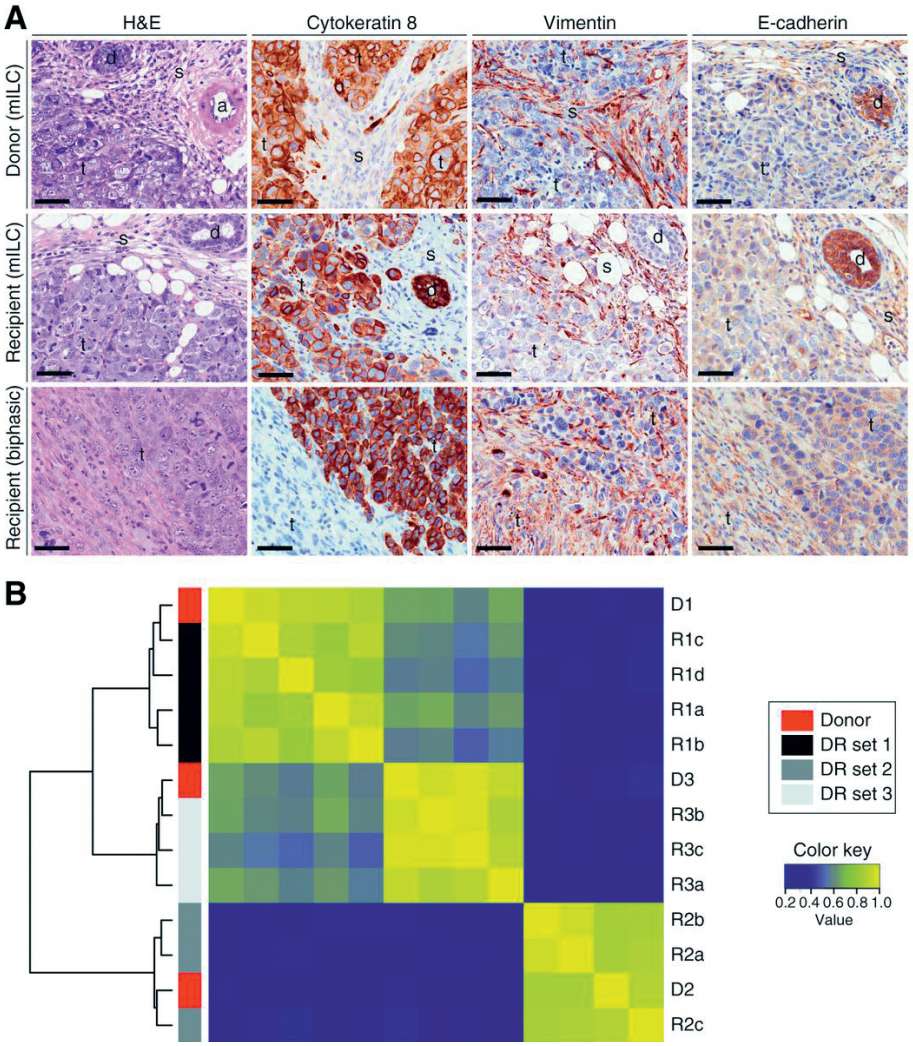

Figure 2. Recipient mice develop pleiomorphic mILCs that recapitulate the histopathologic and molecular characteristics of the parental *K14cre;Cdh1*$^{F/F}$*;Trp53*$^{F/F}$-derived donor tumor. A, representative images of donor (top row) and recipient mammary tumors (middle and bottom rows) characterized by histopathologic and immunohistochemical stainings including cytokeratin 8 (CK8), vimentin, and E-cadherin. The first 2 rows show typical mILCs characterized by positive CK8 staining while negative for vimentin and E-cadherin. Bottom, shows a biphasic tumor composed of epithelial (CK8^{+}) and mesenchymal (CK8^{-}) areas. Note the normal mammary ducts, which serve as internal controls (a, arteriole; d, normal mammary duct; s, stroma; t, mammary tumor). Scale bar, 50 µm. B, heatmap constructed by hierarchical clustering (average linkage) of aCGH profiles from 3 independent sets of paired donor and recipient mammary tumors. Using smoothed genomic profiles, the correlation distance (1−correlation) between all donor and recipient mammary tumors was calculated. [DR set, collection of mammary tumors consisting of one K14cre;Cdh1F/F;Trp53F/F derived donor mILC (D, donor tumor; number refers to the donor) and 3 to 4 related recipient tumors (R, recipient tumor; number refers to the related donor; letter refers to the individual recipient)].

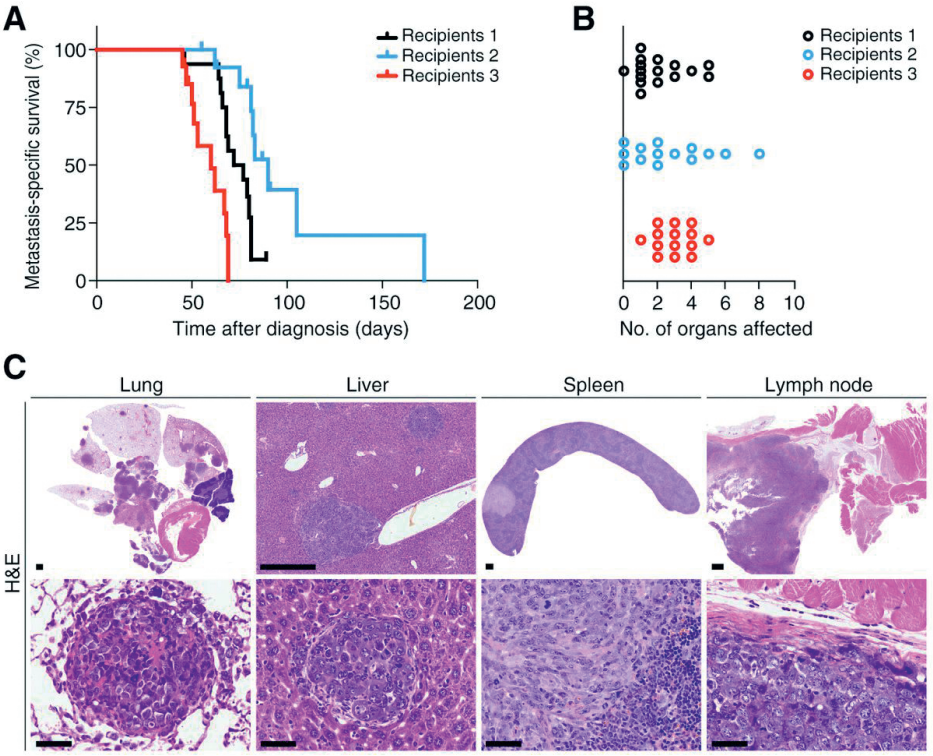

Figure 3. Recipient animals spontaneously develop widespread, clinically overt metastatic disease in various organs. A, Kaplan–Meier metastasis-specific survival curves of recipient mice orthotopically transplanted with tumor fragments from 3 independent *K14cre;Cdh1*$^{F/F}$*;Trp53*$^{F/F}$-derived mILCs. An event is defined as an animal that was sacrificed because of clinical signs of metastatic disease. Censored cases (n = 12/44) indicate mice sacrificed due to locally relapsing tumors reaching a size of approximately 15 × 15 mm. In total, 13 of 16 (recipients 1), 8 of 14 (recipients 2), and 11 of 14 (recipients 3) recipient mice succumbed to clinically overt metastatic disease. B, organs collected from recipient mice were microscopically analyzed for the presence of metastatic foci. The number of organs affected by metastatic disease was quantified per animal (each depicted as one circle). C, representative low (top) and high (bottom) power microscopic images of organs most frequently affected by metastatic disease. Top, scale bar, 500 µm; bottom, scale bar, 50 µm.

To further assess the extent and distribution of metastatic spread in our model, we microscopically analyzed organs isolated from recipient mice for the presence of metastatic foci. In 40 of 44 recipient mice, we observed metastatic foci in at least one organ. In 30 of 44 recipients, 2 or more organs were affected by metastatic disease (Fig. 3B). Consistent with our clinical findings, metastases were predominantly observed in lungs and tumor-draining lymph nodes, though liver, spleen, and distant lymph nodes were also frequently affected (Table 1 and Fig. 3C). Furthermore, metastatic lesions were also observed in pancreas, mesenterium, and peritoneum. This pattern of metastatic

spread strongly correlates with the spectrum of organs affected in human ILC, as human ILCs are prone to metastasize to gastrointestinal tract, ovaries, and peritoneum (18). Together, these data show that recipient mILCs vigorously metastasize leading to widespread, clinically overt metastatic disease in a variety of organs.

Table 1. Overview of recipient organs affected by metastatic disease

	Recipients 1 (n = 16)	**Recipients 2 (n = 14)**	**Recipients 3 (n = 14)**	**Total (*N* = 44), (%)**
Visceral organs				
Lungs	15	8	13	36 (82)
Liver	2	5	1	8 (18)
Spleen	2	4	3	9 (20)
Pancreas	0	2	0	2 (5)
Mesenterium	2	3	2	7 (16)
Peritoneum	0	2	3	5 (11)
Lymph nodes				
Axillary[a]	6	7	11	24 (55)
Mesenteric	1	1	3	5 (11)
Renal	3	5	4	12 (27)
Caudal	2	1	2	5 (11)

[a]Tumor-draining lymph nodes

Metastatic dissemination occurs spontaneously and is not instigated by surgical manipulation of the primary tumor

We aimed for a model in which metastatic dissemination occurs spontaneously. Yet, we could not exclude the possibility that metastatic disease in our model was inadvertently initiated by shedding cancer cells during surgical manipulation of the primary tumor. We reasoned that if metastatic dissemination was exclusively initiated by surgery-induced shedding of cancer cells, the occurrence of metastatic disease would be determined by the time of mastectomy. As a consequence, metastasis-specific survival after surgery would be similar for mice that undergo surgery at different time points in tumor development. Furthermore, surgery-induced shedding of cancer cells would be independent of the size of the resected primary tumor. To test these hypotheses, we conducted a mastectomy at different time points during tumor development and surgically resected recipient tumors that reached a size of 5 × 5, 10 × 10, or 15 × 15 mm (Fig. 4A). Surgical resection of mammary tumors at a size of 10 × 10 mm or more led to

metastatic disease in all animals, whereas mastectomy at a tumor size of 5 × 5 mm led to metastatic disease in only 55% of the animals (Fig. 4B). Interestingly, irrespective of the size of a resected tumor and the time of surgery, the interval between diagnosis of the primary tumor and the occurrence of clinically overt metastatic disease remained similar for mice that succumbed to metastatic disease (Fig. 4B). These data suggest that metastatic dissemination occurs around the time that a primary tumor reaches a size of approximately 5 × 5 mm. To ensure that metastatic dissemination was not inadvertently initiated by shedding cancer cells during surgery, we reanalyzed these data and focused on the interval between surgery and the occurrence of metastatic disease. Metastasis-specific survival after surgery was inversely related to the time of surgery and the size of a resected tumor (Fig. 4C). Thus, these data suggest that metastatic dissemination in our model occurs spontaneously and is not initiated by surgery-induced shedding of cancer cells. However, these data do not exclude the possibility that surgical manipulation of the primary tumor contributes to metastatic dissemination of cancer cells.

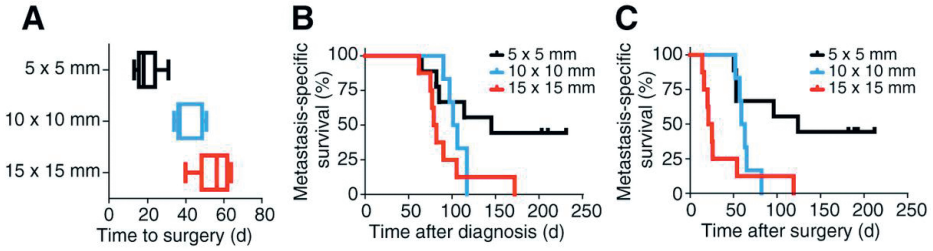

Figure 4. Metastatic dissemination is not instigated by surgical manipulation of mammary tumors. Recipient mice transplanted with donor mILC 2 underwent a mastectomy once mammary tumors reached a size of 5 × 5, 10 × 10, or 15 × 15 mm (n = 9, n = 6, and n = 8 per group, respectively). A, box plots representing the time [mean ± 95% confidence intervals (CI)] from diagnosis to surgical resection of the mammary tumor at the intended size. B, Kaplan–Meier metastasis-specific survival curves of the same recipient mice as described in A. An event is defined as an animal that was sacrificed because of clinical signs of metastatic disease. Censored cases indicate mice that remained healthy till termination of the experiment. Animals that developed locally relapsing tumors were excluded from the analysis. C, Kaplan–Meier metastasis-specific survival curves of the data presented in B, but t = 0 was redefined as the time of surgery. d, days.

Metastatic foci in distant organs strongly resemble histopathologic and genomic characteristics of the parental tumor

To explore the relationship between recipient mammary tumors and their distant metastases, we characterized metastases by morphologic, immunohistochemical, and aCGH analyses and compared them with the parental recipient tumor. Metastatic foci were morphologically similar to epithelial regions within the corresponding recipient

mammary tumor and expressed CK8, but not vimentin or E-cadherin (Fig. 5A). These findings suggest that metastatic foci are either exclusively seeded by epithelial-like cancer cells or that both epithelial- and mesenchymal-like cancer cells metastasize and eventually remain or transform to epithelial cells by a process known as mesenchymal-to-epithelial transition. Similar to parental recipient tumors, metastatic foci also showed abundant immune cell infiltrations (Fig. 5B).

To investigate the genomic relationship between recipient mammary tumors and their metastases, we conducted aCGH and analyzed genomic profiles of paired primary tumors and distant metastases (Supplementary Fig. S3). Unsupervised hierarchical clustering of genomic profiles revealed that local tumors and their distant metastases cluster according to the parental donor tumor (Fig. 5C). Within these clusters, neither recipient mammary tumors and their corresponding metastases nor site-specific lesions (i.e., mammary tumors, lymph node, and lung metastases) could be separated (Fig. 5C). Thus, these data show that genomic profiles of clonally related recipient tumors are highly conserved in regional and distant metastases and that few genomic alterations occur during transition from a primary tumor to a distant site. To more thoroughly examine potential site-specific alterations, we constructed so-called “delta-profiles” and calculated the difference between the genomic profile of a recipient mammary tumor and its paired lymph node or lung metastasis. Though we detected some differences, we did not observe recurrent site-specific alterations in genomic profiles of lymph node or lung metastases (Supplementary Fig. S4). Thus, these data show that recipient mammary tumors and distant metastases exhibit similar genomic profiles and that if copy number changes occurred, they did not recur in independent samples.

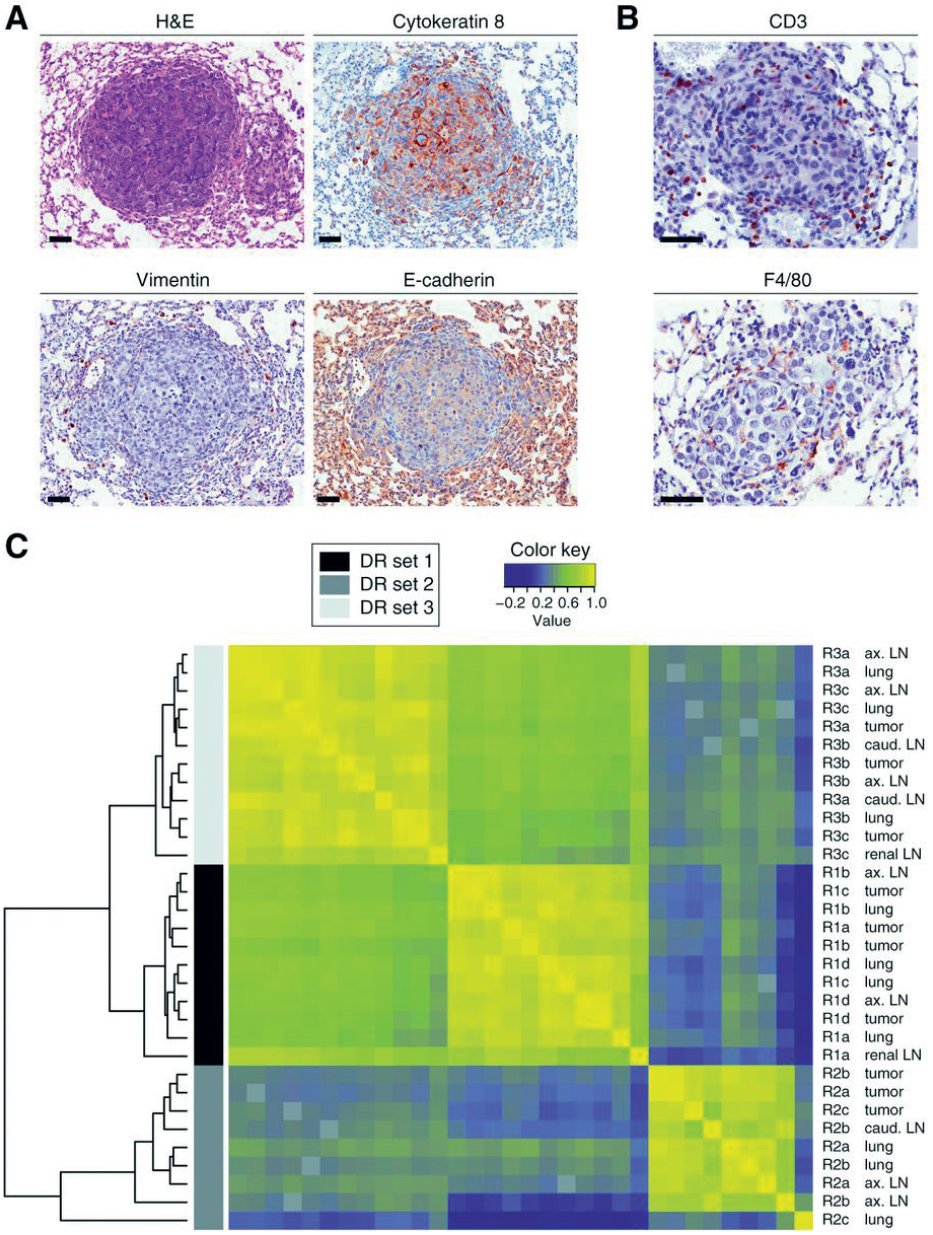

Figure 5. Distant metastatic foci recapitulate the histopathologic and molecular characteristics of the parental recipient mammary tumor. A, histopathologic and immunohistochemical characterization of metastatic foci. Representative images from lung metastases observed in a recipient transplanted with donor mILC 1 are shown. B, infiltration of metastatic foci by $CD3^+$ T-lymphocytes and $F4/80^+$ macrophages (brown staining). Scale bar, 50 µm. C, heatmap constructed by hierarchical clustering (average linkage) of genomic profiles from 10 sets (3–4 sets per donor) of recipient tumors and paired lymph node and lung metastases. Using smoothed genomic profiles, the correlation distance (1−correlation) between recipient

mammary tumors and metastases was calculated. [DR set, paired sets (indicated by lower case letters) of donor-related (indicated by numbers) recipient mammary tumors and their local and/or distant metastases. R, recipient tissue; ax. LN, axillary, tumor-draining lymph node metastasis; caud. LN, caudal lymph node metastasis; lung, lung metastasis; renal LN, renal lymph node metastasis; tumor, primary mammary tumor].

Mammary tumors and distant metastases exhibit similar therapeutic profiles upon (neo-) adjuvant treatment with standard-of-care chemotherapeutics

To study chemotherapy responses of clonally related mammary tumors and distant microscopic metastases, we generated a cohort of recipient mice transplanted with the same donor tumor. Tumor-bearing recipients were then assigned to adjuvant or neoadjuvant treatments with PBS (control), doxorubicin, or docetaxel. In both settings, treatments were administered once weekly for a fixed period of 4 weeks (Fig. 6A). Neoadjuvant treatments initiated at a tumor size of 5 × 5 mm resulted in marked stasis in tumor development. However, tumors rapidly regained growth after completion of the treatment (Fig. 6B). Consequently, neoadjuvant-treated animals that underwent a mastectomy at a tumor size of 15 × 15 mm eventually succumbed to metastatic disease (Fig. 6C and D). Likewise, adjuvant chemotherapy treatments targeting clinically undetectable microscopic metastases were initiated 3 days after mastectomy and led to an initial but temporary response resulting in a clear increase in metastasis-specific survival (Fig. 6C and D). Consistent with observations in human invasive lobular carcinoma (22), these data show that (neo-) adjuvant treatments with doxorubicin and docetaxel result in a survival benefit, but do not give rise to a durable, complete response. Furthermore, treatment-associated survival benefits for adjuvant and neoadjuvant treated cohorts suggest that mammary tumors and distant metastases exhibit similar therapeutic profiles upon neoadjuvant or adjuvant treatment with the standard-of-care chemotherapeutics doxorubicin and docetaxel.

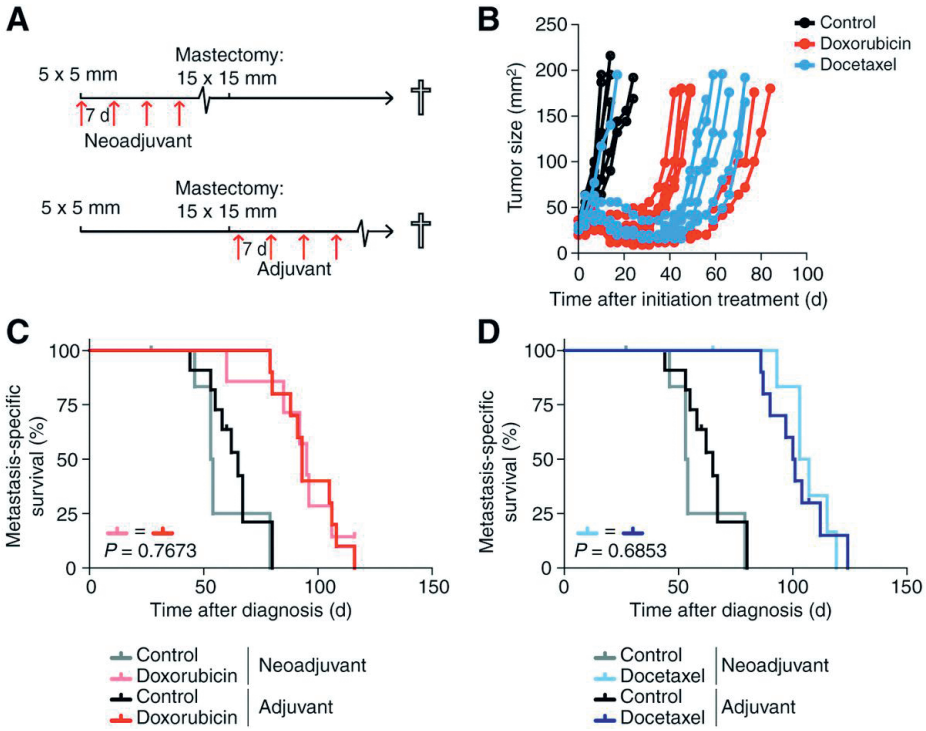

Figure 6. Clonally related recipient tumors and distant metastases respond similarly to neoadjuvant and adjuvant treatment with standard-of-care chemotherapeutics. A, schematic overview of neoadjuvant and adjuvant chemotherapy treatments in tumor-bearing recipients transplanted with the same donor tumor. Neoadjuvant and adjuvant treatments with PBS (control), doxorubicin, or docetaxel were administered once weekly for a fixed period of 4 weeks. Neoadjuvant treatments were initiated at a tumor size of 5 × 5 mm, whereas adjuvant treatments were started 3 days after mastectomy. Mammary tumors were surgically resected at a size of approximately 15 × 15 mm and mice were sacrificed once they developed clinical signs of metastatic disease. B, individual tumor growth curves of recipient mice that received neoadjuvant treatment with PBS (black), doxorubicin (red), or docetaxel (blue; n = 7/treatment). C and D, Kaplan–Meier metastasis-specific survival curves of recipient mice that underwent neoadjuvant (n = 7/treatment) or adjuvant treatment (n = 10–11/treatment) with PBS (C and D), doxorubicin (C) or docetaxel (D). An event is defined as an animal that was sacrificed due to clinical signs of metastatic disease. Censored cases indicate mice sacrificed because of locally relapsing tumors reaching a size of approximately 15 × 15 mm. Statistical analyses were conducted using the log-rank test to compare neoadjuvant versus adjuvant doxorubicin and docetaxel treatments. d, days.

DISCUSSION

In this study, we have developed a preclinical mouse model of *de novo* breast cancer metastasis formation that recapitulates the key biologic events of the metastatic

cascade and closely mimics the clinical course of metastatic disease in humans. We used the well-characterized conditional *K14cre;Cdh1*$^{F/F}$*;Trp53*$^{F/F}$ mouse model of *de novo* mammary tumor formation that recapitulates several key features of human ILC (14). Exploiting these features, we orthotopically transplanted pleiomorphic *K14cre;Cdh1*$^{F/F}$*;Trp53*$^{F/F}$ derived mILC fragments into wild-type syngeneic recipient mice and found that donor and recipient mammary tumors showed similar histopathologic and molecular traits. We then mimicked the clinical setting and surgically resected established recipient tumors. Thus, we were able to extend the life span of recipient animals, thereby allowing disseminated cancer cells to prosper and establish advanced distant metastases. As a result, recipient mice eventually succumbed to widespread clinically overt metastatic disease in lymph nodes, lungs, and gastrointestinal tract. Extensive analysis of metastatic foci revealed that metastases maintained their mILC-like phenotype and that metastases were genomically hardly distinguishable from clonally related recipient mammary tumors. Neoadjuvant interventions studies with standard-of-care chemotherapeutics further revealed that clonally related recipient tumors and distant metastases exhibited very similar therapeutic profiles.

On the basis of these results, we believe that our model provides a valuable tool to study metastatic dissemination in invasive lobular breast cancer and offers several advantages over most of the currently available metastasis models. First, metastatic dissemination in our model is not induced by intravenous injection of cancer cells, but occurs spontaneously by seeding cancer cells from orthotopically transplanted tumors. Thus, metastatic dissemination in this model more closely reflects the key biologic events of the metastatic cascade. Furthermore, recipient mammary tumors in our model were not established by orthotopic transplantation of cancer cells derived from *in vitro* maintained cancer cell lines. Cancer cell line–based metastasis models have several advantages, as tumor cells are easily manipulated for mechanistic studies. Likewise, introduction of biomarkers for *in vivo* noninvasive imaging of disease progression is relatively straightforward. Yet, cell line–based metastasis models have their limitations, as *in vitro* maintained cancer cell lines fail to retain the cellular heterogeneity present in the parental tumor (13). As this heterogeneity reflects a diverse composition of distinct subclones within a primary tumor, loss of biologic variation could have important implications for metastatic behavior and therapy responses observed in these models (23). To circumvent these limitations, we orthotopically transplanted tumor fragments derived from *de novo K14cre;Cdh1*$^{F/F}$*;Trp53*$^{F/F}$ mILCs into wild-type hosts. Thus, we were able to reconstitute equally heterogeneous recipient mammary tumors. As a consequence, recipient mammary tumors in our model are more likely to

reflect the heterogeneity also observed in human cancer (24, 25). Though more realistic, it is important to note that this biologic variety comes at the expense of experimental flexibility as tumors are more difficult to manipulate.

Second, by transplanting mILC fragments into syngeneic hosts, we were able to reconstitute mammary tumors in the context of a functional, immune-proficient microenvironment. Therefore, our model can be used to address the role of the immune system in breast cancer metastasis formation. This is essential because accumulating evidence indicates that immune cells and their soluble mediators modulate the process of metastatic spread both at the level of the primary tumor as well as at distant sites (4, 26). Furthermore, as this system permits easy manipulation of the stromal compartment by transplanting tumor fragments into hosts with altered stromal traits, it can also be used to assess the functional involvement of other cancer cell extrinsic factors.

Third, unlike in other models (27), metastatic disease in our model is not confined to a limited set of distant sites, but encompasses a variety of lymphoid and visceral organs. The common involvement of tumor-draining and distant lymph nodes suggests that metastatic spread in our model occurs at least partially by spontaneous lymphatic dissemination of cancer cells. In contrast to some other models, this pattern of metastatic dissemination arises spontaneously and does not require *in vivo* enrichment, selection, and reinjection of cancer cells. Moreover, the distribution of organs affected by metastatic disease in our model is highly reminiscent to the metastatic spectrum observed in human invasive lobular breast cancer (18). Thus, based on these merits, our model presumably more closely reflects the biology of organ-specific metastatic colonization. Because various organs are often affected simultaneously, this model allows a careful, paired analysis of metastases arising in different anatomical locations as illustrated by our genomic studies. Extending these studies by an in-depth comparison of metastatic foci to their parental tumor paves the way to gain new insights into mechanisms regulating organ-specific metastasis formation.

Fourth, metastatic dissemination in our model led to clinically overt metastatic disease thus allowing us to determine metastasis-specific survival based on clinically defined endpoints. These clinically defined endpoints provide a more precise estimation of disease burden, as number, size and cumulative area of metastatic foci not necessarily correlate with the disturbance of organ function. For example, solely based on their critical location, only few lung metastases might lead to a rapid deterioration in respiratory capacity. Likewise, pleural effusions commonly observed in lung metastases-bearing animals have a profound impact on respiratory capacity. Ultimately, these factors collectively result in organ failure leading to clinical signs of respiratory distress.

As a result, clinical signs of metastatic disease and related metastasis-specific survival more precisely reflect the disease burden as they incorporate all the aforementioned factors.

Finally, given its penetrant and predictive metastatic phenotype, our model can also be used as a preclinical tool to test (novel) therapeutic agents targeting metastatic disease (27). As shown by our chemotherapy intervention experiments, these studies can either be conducted in an adjuvant or neoadjuvant setting, thus allowing a careful and independent evaluation of therapeutic agents targeting the primary tumor and low-volume microscopic or advanced metastatic disease. Neoadjuvant and adjuvant intervention studies in cohorts of mice transplanted with the same donor tumor can be combined to create a well-controlled experimental setting that allows a reproducible, pair-wise comparison of therapy efficacy in clonally related mammary tumors and distant metastases. Observations in one cohort of recipient mice can subsequently be validated in a second cohort of mice transplanted with an independent donor tumor. If intertumor heterogeneity between independent *K14cre;Cdh1*$^{F/F}$*;Trp53*$^{F/F}$ donor tumors gives rise to different responses, this approach can also be exploited to study the impact of naturally occurring donor-specific genomic aberrations on (organ-specific) metastasis formation and therapy response. It is, however, important to note that recipient mammary tumors in this model are derived from end-stage mammary donor tumors. Therefore, our model potentially underestimates the contribution of early disseminated cancer cells, which, based on their independent and potentially divergent somatic evolution, might have an impact on the observed therapeutic profiles (28). Another drawback of our system is the current lack of markers for *in vivo* noninvasive imaging of metastatic disease. However, this issue can be resolved by the introduction of bioluminescence or fluorescence imaging reporters in donor mice.

In conclusion, we successfully developed a preclinical mouse model of *de novo* breast cancer metastasis formation that maintains and exploits the unique features of the original *K14cre;Cdh1*$^{F/F}$*;Trp53*$^{F/F}$ model while simultaneously circumventing its limitations by conducting a mastectomy to prevent premature tumor-associated loss of recipient mice. We believe that this model provides a valuable tool to study the biology of metastatic disease and to evaluate the efficacy of (novel) therapeutic agents targeting metastatic disease. Our experimental approach can be applied to similar mouse models of *de novo* tumorigenesis, thus yielding a broader availability of mouse models that faithfully recapitulate metastatic disease in humans. Together, these models are likely to provide new insights that will support the development of more effective treatment strategies and may therefore benefit many patients suffering from metastatic disease.

DISCLOSURE OF POTENTIAL CONFLICTS OF INTEREST

No potential conflicts of interest were disclosed.

AUTHORS' CONTRIBUTIONS

Conception and design: M.W. Hollmann, J. Jonkers, K.E. de Visser

Development of methodology: C.W. Doornebal, M.W. Hollmann, J. Jonkers, K.E. de Visser

Acquisition of data (provided animals, acquired and managed patients, provided facilities, etc.): C.W. Doornebal, S. Klarenbeek, T.M. Braumuller, C.-S. Hau

Analysis and interpretation of data (e.g., statistical analysis, biostatistics, computational analysis): C.W. Doornebal, S. Klarenbeek, C.N. Klijn, M. Ciampricotti, M.W. Hollmann, J. Jonkers, K.E. de Visser

Writing, review, and/or revision of the manuscript: C.W. Doornebal, C.N. Klijn, M.W. Hollmann, J. Jonkers, K.E. de Visser

Administrative, technical, or material support (i.e., reporting or organizing data, constructing databases): C.W. Doornebal, S. Klarenbeek, T.M. Braumuller, M. Ciampricotti, C.-S. Hau, M.W. Hollmann

Study supervision: M.W. Hollmann, K.E. de Visser

GRANT SUPPORT

This research was supported by grants from the Dutch Cancer Society (KWF grants 2006-3715 and 2011-5004 to K.E. de Visser and J. Jonkers), the Netherlands Organization for Scientific Research (NWO grant VIDI 917.96.307 to K.E. de Visser), the Association for International Cancer Research (AICR grant 11-0677 to K.E. de Visser), and the NWO-funded Cancer Systems Biology Center (CSBC).

The costs of publication of this article were defrayed in part by the payment of page charges. This article must therefore be hereby marked advertisement in accordance with 18 U.S.C. Section 1734 solely to indicate this fact.

ACKNOWLEDGMENTS

The authors thank technical assistance from the Laboratory Animal Department, Animal Pathology Department and Central Microarray Facility at the Netherlands Cancer Institute and the members of the De Visser and Jonkers labs for fruitful discussions and input. The authors also thank Seth Coffelt, Kelly Kersten, and Martine van Miltenburg for critically reading the manuscript.

REFERENCES

1. Gupta GP,Massagué J. Cancer metastasis: building a framework. Cell 2006;127:679–95.
2. Talmadge JE, Fidler IJ. AACR Centennial Series: The biology of cancer metastasis: historical perspective. Cancer Res 2010;70:5649–69.
3. Valastyan S, Weinberg RA. Tumor metastasis: molecular insights and evolving paradigms. Cell 2011;147:275–92.
4. Joyce JA, Pollard JW. Microenvironmental regulation of metastasis. Nat Rev Cancer 2008;9:239–52.
5. Nguyen DX, Bos PD, Massagué J. Metastasis: from dissemination to organ-specific colonization. Nat Rev Cancer 2009;9:274–84.
6. Müller A, Homey B, Soto H, Ge N, Catron D, Buchanan ME, et al. Involvement of chemokine receptors in breast cancer metastasis. Nature 2001;410:50–56.
7. Hiratsuka S, Nakamura K, Iwai S, Murakami M, Itoh T, Kijima H, et al. MMP9 induction by vascular endothelial growth factor receptor-1 is involved in lung-specific metastasis. Cancer Cell 2002;2:289–300.
8. Kaplan RN, Riba RD, Zacharoulis S, Bramley AH, Vincent L, Costa C, et al. VEGFR1-positive haematopoietic bone marrow progenitors initiate the premetastatic niche. Nature 2005;438:820–7.
9. Kaplan RN, Rafii S, Lyden D. Preparing the “Soil”: the premetastatic niche. Cancer Res 2006;66:11089–93.
10. Fantozzi A, Christofori G. Mouse models of breast cancer metastasis. Breast Cancer Res 2006;8:212.
11. Jonkers J, Derksen PWB. Modeling metastatic breast cancer in mice. J Mammary Gland Biol Neoplasia 2007;12:191–203.
12. Francia G, Cruz-Munoz W, Man S, Xu P, Kerbel RS. Mouse models of advanced spontaneous metastasis for experimental therapeutics. Nat Rev Cancer 2011;11:135–41.
13. Keller PJ, Lin AF, Arendt LM, Klebba I, Jones AD, Rudnick JA, et al. Mapping the cellular and molecular heterogeneity of normal and malignant breast tissues and cultured cell lines. Breast Cancer Res 2010;12:R87.
14. Derksen PWB, Liu X, Saridin F, van der Gulden H, Zevenhoven J, Evers B, et al. Somatic inactivation of E-cadherin and p53 in mice leads to metastatic lobular mammary carcinoma through induction of anoikis resistance and angiogenesis. Cancer Cell 2006;10:437–449.
15. Rottenberg S, Nygren AOH, Pajic M, Leeuwen V, B FW, Van Der Heijden I, et al. Selective induction of chemotherapy resistance of mammary tumors in a conditional mouse model for hereditary breast cancer. Proc Natl Acad Sci U S A 2007;104:12117–22.
16. Klijn C, Holstege H, de Ridder J, Liu X, Reinders M, Jonkers J, et al. Identification of cancer genes using a statistical framework for multi-experiment analysis of nondiscretized array CGH data. Nucleic Acids Res 2008;36:e13.
17. de Ronde JJ, Klijn C, Velds A, Holstege H, Reinders MJ, Jonkers J, et al. KC-SMARTR: An R package for detection of statistically significant aberrations in multi-experiment aCGH data. BMC Res Notes 2010;3:298.

18. Arpino G, Bardou VJ, Clark GM, Elledge RM. Infiltrating lobular carcinoma of the breast: tumor characteristics and clinical outcome. Breast Cancer Res 2004;6:R146–56.
19. Leek RD, Lewis CE, Whitehouse R, Greenall M, Clarke J, Harris AL. Association of macrophage infiltration with angiogenesis and prognosis in invasive breast carcinoma. Cancer Res 1996;56:4625–9.
20. Tsutsui S, Yasuda K, Suzuki K, Tahara K, Higashi H, Era S. Macrophage infiltration and its prognostic implications in breast cancer: the relationship with VEGF expression and microvessel density. Oncol Rep 2005;14:425–31.
21. DeNardo DG, Barreto JB,AndreuP, Vasquez L, Tawfik D, Kolhatkar N, et al. $CD4^+$ T cells regulate pulmonary metastasis of mammary carcinomas by enhancing protumor properties of macrophages. Cancer Cell 2009;16:91–102.
22. Cristofanilli M, Gonzalez-Angulo A, Sneige N, Kau S-W, Broglio K, Theriault RL, etal. Invasive lobular carcinoma classic type: response to primary chemotherapy and survival outcomes. J Clin Oncol 2005;23:41–48.
23. Khanna C, Hunter K. Modeling metastasis in vivo. Carcinogenesis 2005;26:513–23.
24. Marusyk A, Almendro V, Polyak K. Intra-tumour heterogeneity: a looking glass for cancer? Nat Rev Cancer 2012;12:323–34.
25. Gerlinger M, Rowan AJ, Horswell S, Larkin J, Endesfelder D, Gronroos E, et al. Intratumor heterogeneity and branched evolution revealed by multiregion sequencing. N Engl J Med 2012;366:883–92.
26. de Visser KE, Eichten A, Coussens LM. Paradoxical roles of the immune system during cancer development. Nat Rev Cancer 2006;6:24–37.
27. Talmadge JE, Singh RK, Fidler IJ, Raz A. Murine models to evaluate novel and conventional therapeutic strategies for cancer. Am J Pathol 2007;170:793–804.
28. Klein CA.Parallel progression of primary tumours and metastases. Nat Rev Cancer 2009;9:302–312.

SUPPLEMENTARY FIGURES

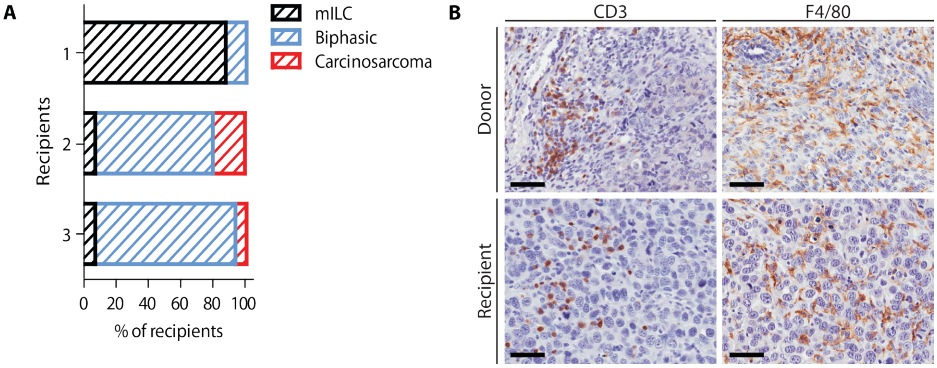

Figure S1. Recipient mice develop pleiomorphic mILCs that are infiltrated by immune cells. (A) Recipient mammary tumors were characterized by immunohistochemistry and classified based on their histological phenotype (n=16, 14 and 14 for recipients 1, 2 and 3 respectively). (B) Like spontaneous *K14cre;Cdh1*$^{F/F}$*;Trp53*$^{F/F}$ derived mammary tumors (upper row), recipient mammary tumors (lower row) are infiltrated by CD3^{+} T-lymphocytes and F4/80^{+} macrophages. Scale bar = 50 µm. Representative images are shown.

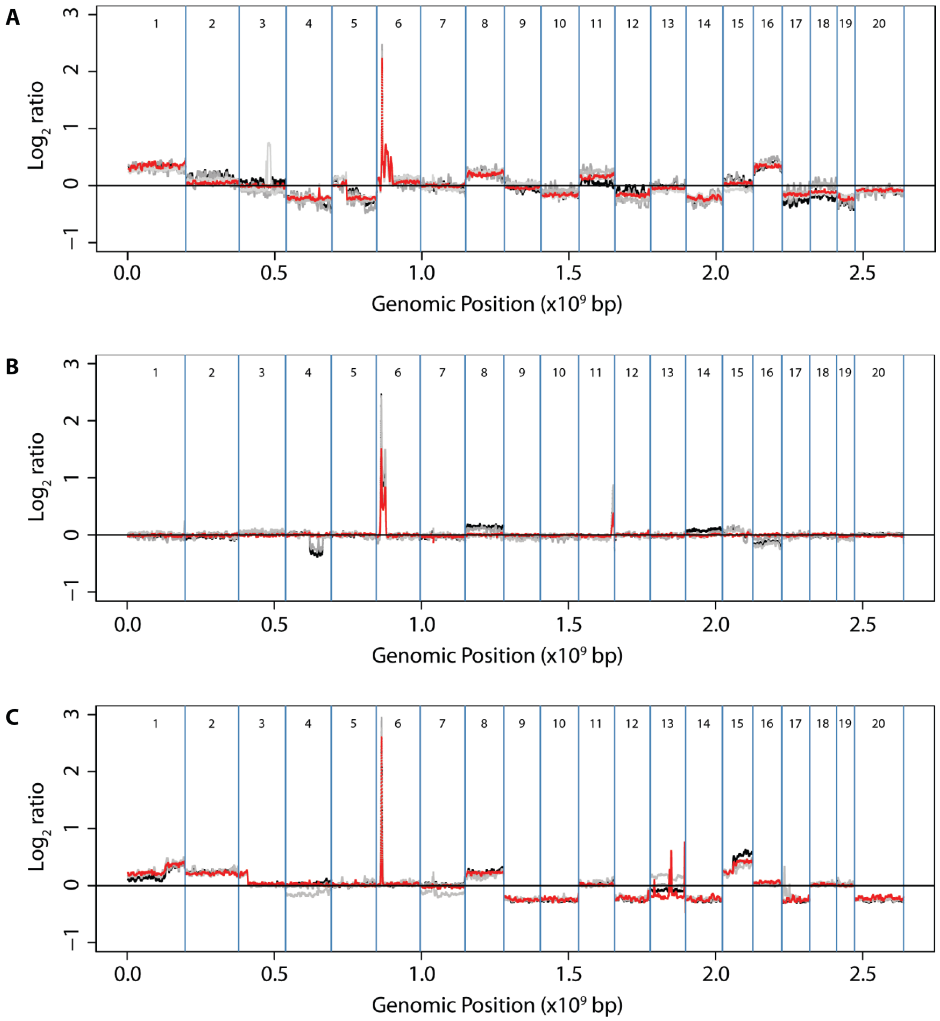

Figure S2. Genomic profiles of *K14cre;Cdh1$^{F/F}$;Trp53$^{F/F}$* derived donor mILCs are highly conserved in transplanted recipient outgrowths. (A-C) Genomic profiles of paired *K14cre;Cdh1$^{F/F}$;Trp53$^{F/F}$* derived donor tumors (red curves, A = donor mILC 1, B= donor mILC 2, C=donor mILC 3) and related recipient outgrowths (grey and black curves, n=3-4 per donor).

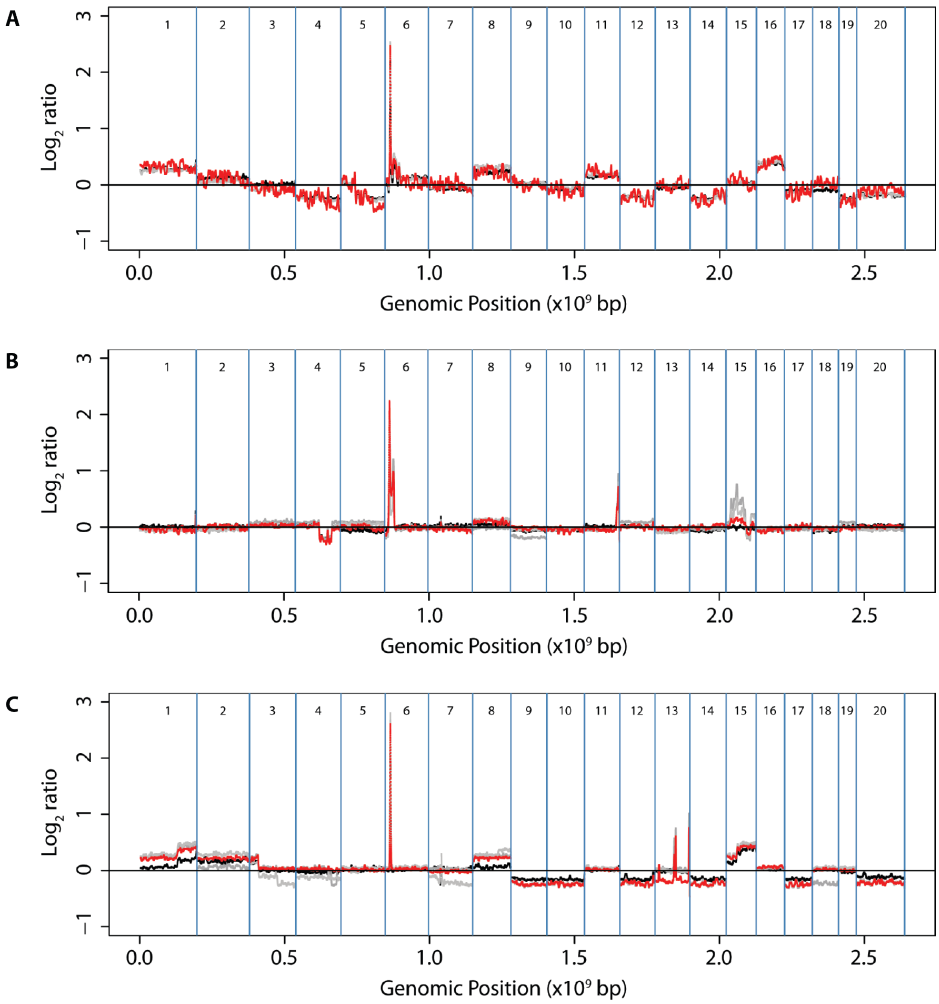

Figure S3. Recipient mammary tumors and distant metastases exhibit very similar genomic profiles. (A-C) aCGH profiles of paired recipient mammary tumors (red curves, A=recipient 1b, B=recipient 2b, C=recipient 3b) and related lung- and lymph node metastases (grey and black curves, n=2-3 per recipient).

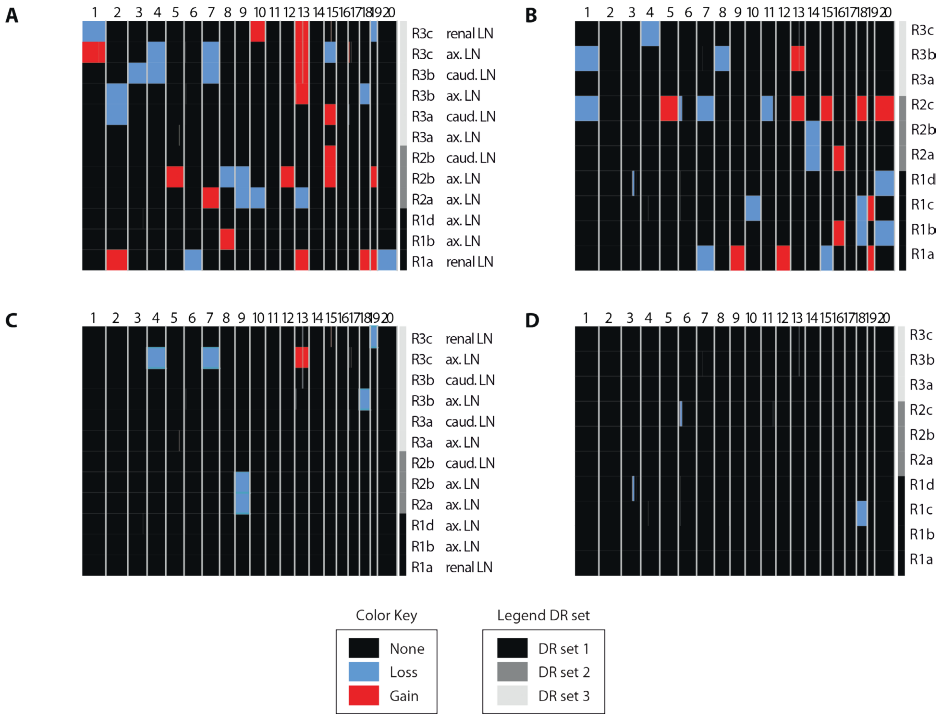

Figure S4. Genomic profiles of paired lung- and lymph node metastases suggest that metastatic dissemination to these organs is not driven by recurrent, tissue specific copy number aberrations. Paired sets (3-4 sets per donor) of recipient mammary tumors and related lymph node- (A&C) or lung metastases (B&D) were analyzed by aCGH. Using quantile normalized genomic profiles, we directly compared paired genomic profiles by computing so-called 'delta-profiles' and subtracting the genomic profiles of recipient mammary tumors from their related metastases. Delta-profiles were then segmented and segments which exceeded an absolute value of 0.1 (A&B) or 0.2 (C&D) were plotted per chromosome. (DR set, paired sets (indicated by lower case letters) of donor-related (indicated by numbers) recipient mammary tumors and their metastases. R, recipient tissue; ax. LN, axillary lymph node metastasis; caud. LN, caudal lymph node metastasis; lung, lung metastasis; renal LN, renal lymph node metastasis; tumor, primary mammary tumor).

Table S1. Detailed information about antibodies and antigen retrieval methods used in immunohistochemical experiments.

Antibody	*Clone (company)*	*Dilution*	*Incubation time/ temperature*	*Antigen retrieval method*
Rat α-mouse cytokeratin 8	TROMA-1 (University of Iowa[1])	1:600	ON	Citra buffer (Biogenex[2])
Guinea pig α-mouse Vimentin	20R-VP004 (Fitzgerald[3])	1:1500	5hr at RT, then ON at 4°C	Prot. K
Mouse α-mouse E-cadherin	36/E-cadherin (BD Biosciences[4])	1:400	ON	Tris/EDTA, pH 9.0
Rabbit α-human CD3	SP7 (Neomarkers[5])	1:100	ON	Citra buffer (Biogenex[2])
Rat α-mouse F4/80	CI:A3-1 (Serotec[6])	1:400	ON	None
Mouse α-BrdU	Bu20A (Dako[7])	1:100	ON	Citra buffer (Biogenex[2])
Biotinylated goat α-rat	(Santa Cruz[8])	1:100	30 min. at RT	NA
Biotinylated goat α-mouse	(Dako[7])	1:500	30 min. at RT	NA
Biotinylated goat α-guinea pig	(Jackson Immunoresearch[9])	1:750	30 min. at RT	NA

[1] Iowa City, Iowa, USA

[2] San Ramon, CA, USA

[3] Concord, MA, USA

[4] San Diego, CA, USA

[5] Fremont, CA, USA

[6] Düsseldorf, Germany

[7] Glostrup, Denmark

[8] Santa Cruz, CA, USA

[9] Westgrove, PA, USA

SUPPLEMENTARY METHODS

Array comparative genomic hybridization (aCGH)

Genomic DNA from fresh-frozen primary tumors, metastases and spleens was isolated by phenol- chloroform extraction. Methods of DNA labeling, array construction, hybridization, array normalization and data analysis have been described previously (1). Briefly, genomic DNA isolated from primary tumors, metastases and spleens was randomly fragmented by acoustic shearing using the Covaris S2

System (Covaris Inc., Woburn, MA, USA). Samples were then random-prime labeled with Cy3 and Cy5 dyes and co-hybridized to Mouse CGH 12x385K Whole-Genome microarrays (Roche NimbleGen Inc., Madeson, WI, USA) using the corresponding donor spleen DNA as a reference. Arrays were scanned at 532nm (Cy3) and 635nm (Cy5) using an MS200 Microarray Scanner (Roche NimbleGen Inc., Madeson, WI, USA) and data were extracted using NimbleScan software. Background corrected log2 ratios derived from the NimbleScan analysis were used for all further analyses. Raw data have been deposited in NCBI's GEO repository and are accessible through GEO Series accession number GSE34666.

Clustering analysis aCGH profiles

A smoothed profile was computed for each sample using the comparative module of the *Kcsmart* package (2, 3) as implemented in the *Bioconductor* toolbox (version 2.8) for the statistical programming language *R*. The kernel size for smoothing was set at $\sigma = 1$ Mb. The correlation distance (1-correlation) between all smoothed tumor and metastases profiles was calculated and hierarchical clustering (average linkage) was used to construct the heatmap.

Analysis of paired aCGH profiles

To allow for a direct comparison of recipient mammary tumors and corresponding lymph node- and/or lung metastases, the dataset was normalized by quantile normalization. The distributions of the data were equally ranged, making these samples directly comparable by profile subtraction without losing information. After normalization, we subtracted the mammary tumor profile from its paired lung- or lymph node metastasis profile, thus creating a so-called 'delta-profile'. These delta profiles were then segmented by the DNAcopy package as implemented in the *Bioconductor* toolbox (version 2.8) for the R statistical programming language. Segmentation parameters were standard, except we used the option to undo a breakpoint call based on standard

deviation. We analyzed segments in the delta profiles whose absolute value exceeded either a 0.1 or 0.2 threshold.

Histology and immunohistochemistry

Collected tumors and tissues were formalin-fixed, paraffin-embedded, sectioned and stained as described previously (4). Briefly, tissues were fixed for 24 h in 10% neutral buffered formalin, embedded in paraffin, sectioned at 4 µm and stained with heamatoxylin and eosin (H&E) for histopathological evaluation. For immunohistochemical analysis, 5 µm thick paraffin sections were cut, deparaffinized and stained. Antibodies and antigen retrieval methods are described in detail in the Table S1. All immunohistochemical staining experiments included negative controls to determine background staining, which was negligible. Stained slides were digitally processed using the Aperio ScanScope (Aperio, Vista, CA, USA) and captured using ImageScope software version 11.0.2 (Aperio). Data shown are representative results obtained from a minimum of 3 recipient mice per donor.

REFERENCE LIST

(1) Selzer RR, Richmond TA, Pofahl NJ, Green RD, Eis PS, Nair P, et al. Analysis of chromosome breakpoints in neuroblastoma at sub-kilobase resolution using fine-tiling oligonucleotide array CGH. Genes Chromosomes Cancer 2005;44:305-19.

(2) Klijn C, Holstege H, de RJ, Liu X, Reinders M, Jonkers J, et al. Identification of cancer genes using a statistical framework for multiexperiment analysis of nondiscretized array CGH data. Nucleic Acids Res 2008;36:e13.

(3) de Ronde JJ, Klijn C, Velds A, Holstege H, Reinders MJ, Jonkers J, et al. KC-SMARTR: An R package for detection of statistically significant aberrations in multi-experiment aCGH data. BMC Res Notes 2010;3:298.

(4) Evers B, Speksnijder EN, Schut E, Ciampricotti M, Smalley MJ, Derksen PW, et al. A tissue reconstitution model to study cancer cell-intrinsic and -extrinsic factors in mammary tumourigenesis. J Pathol 2010;220:34-44.